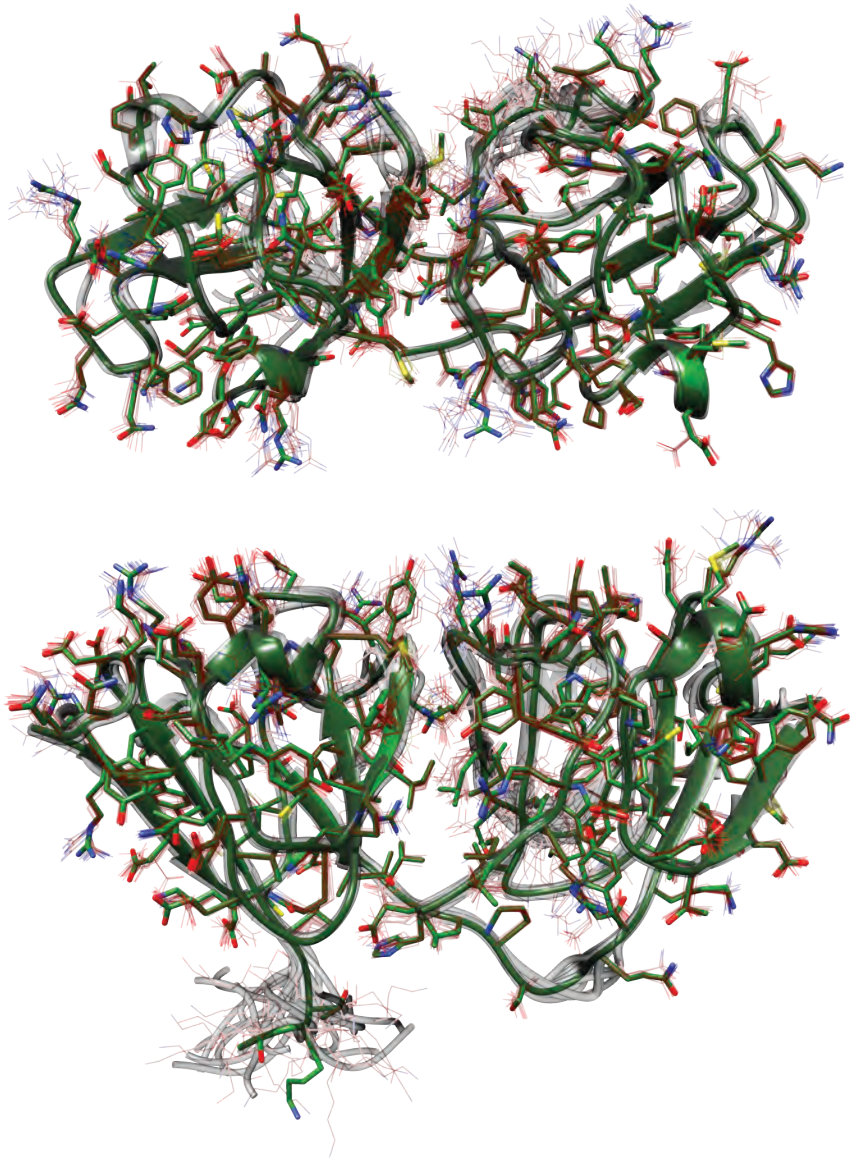

Figure S1: Depiction of the final 20-structure family for γS-WT (transparent grey, colored by heteroatom) and the energy-minimized average NMR structure (opaque green colored by heteroatom), including sidechains. Related to Figure 1 and Table 1.

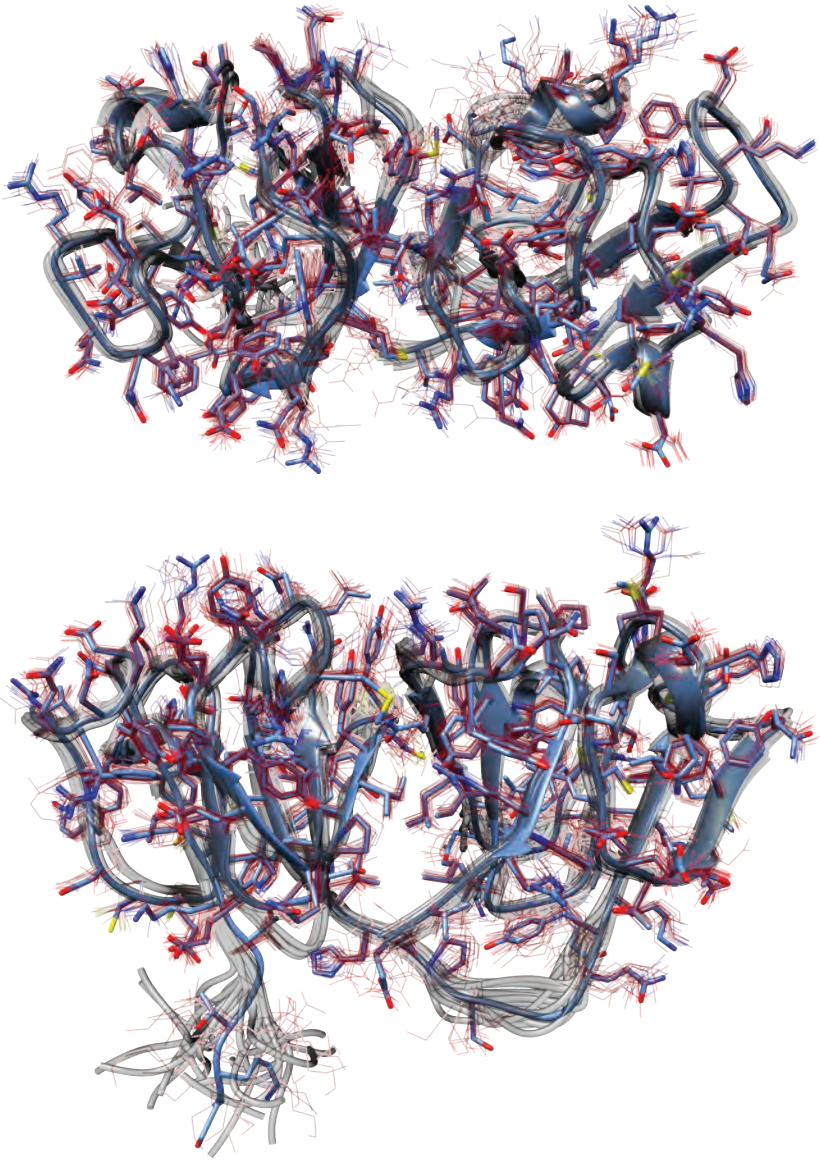

Figure S2: Depiction of the final 20-structure family for γS-G18V (transparent grey, colored by heteroatom) and the energy-minimized average NMR structure (opaque blue colored by heteroatom), including sidechains. Related to Figure 1 and Table 1.

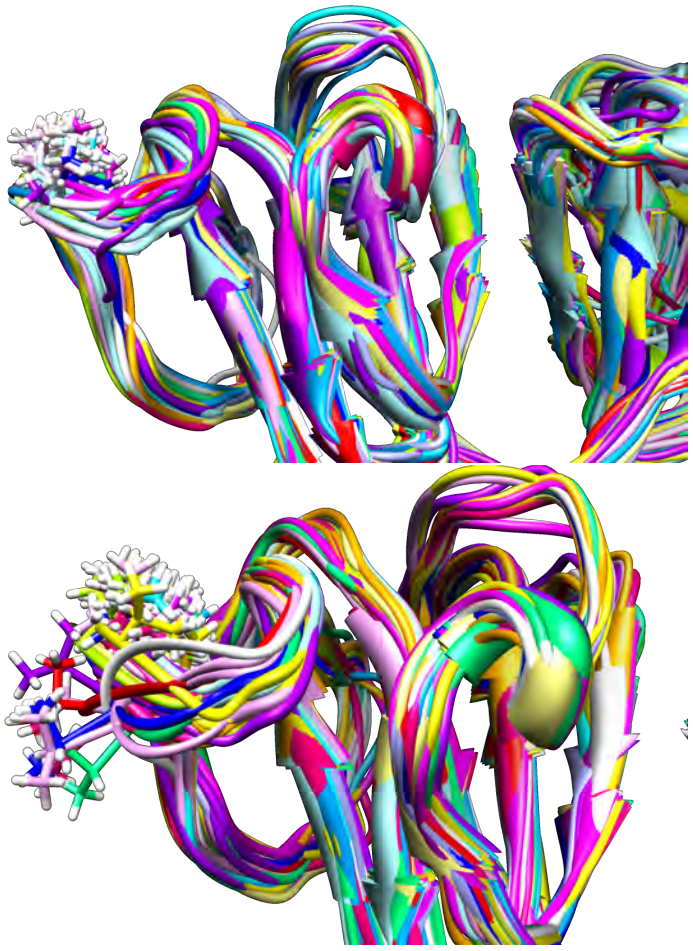

Figure S3: Comparison of two structural refinements without NOE restraints to residues 16-20 and without angular RDC restraints to residue 18 performed with (top) and without (bottom) the angular backbone restraint provided from the HNHA experiment for V18. Note that this single restraint is sufficient to keep V18 in place in all of the top scoring structures. Even if the J-coupling restraint is omitted, only five of 50 calculated structures land with V18 in an "allowed" dihedral angle conformation. Related to Figure 1 and Table 1.

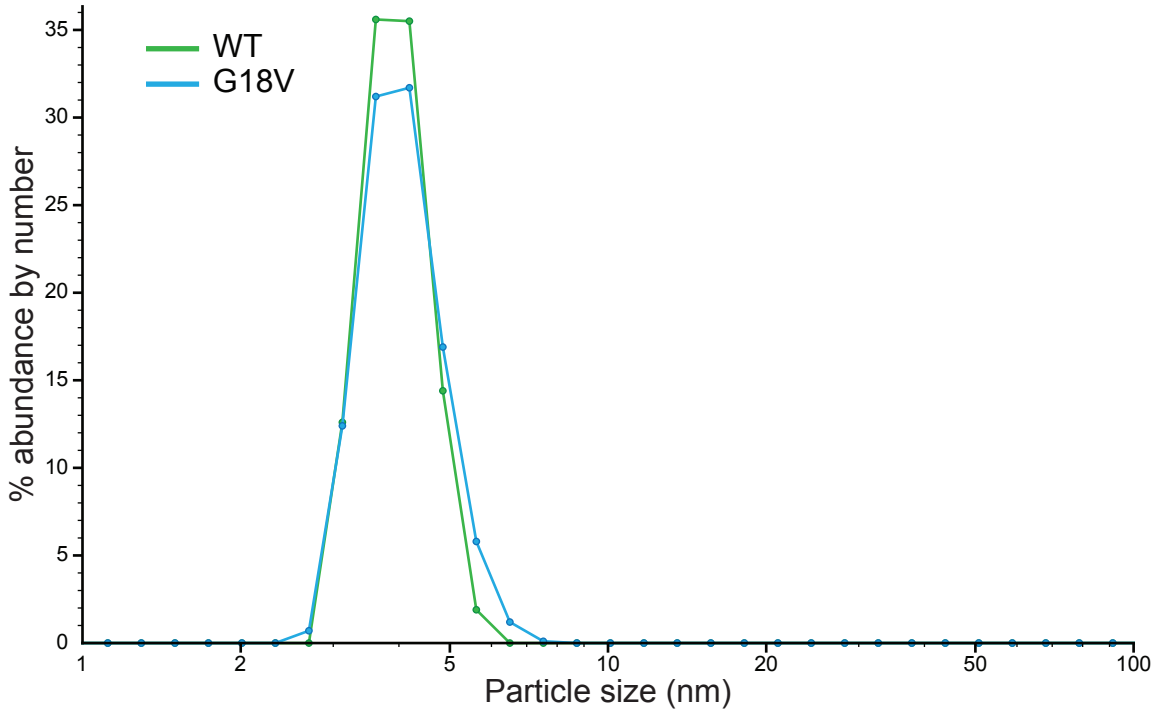

Figure S4: Particle size of γS-WT and γS-G18V at 2.0 mM concentration in 10 mM acetate buffer pH 4.5 measured by dynamic light scattering on a Zetasizer Nano ZS (Malvern Instruments, Ltd.). Under these conditions γS-WT and γS-G18V are fully monomeric, with particle diameters of 39.7 and 40.9 Å respectively. Related to Figure 1 and Table 1.

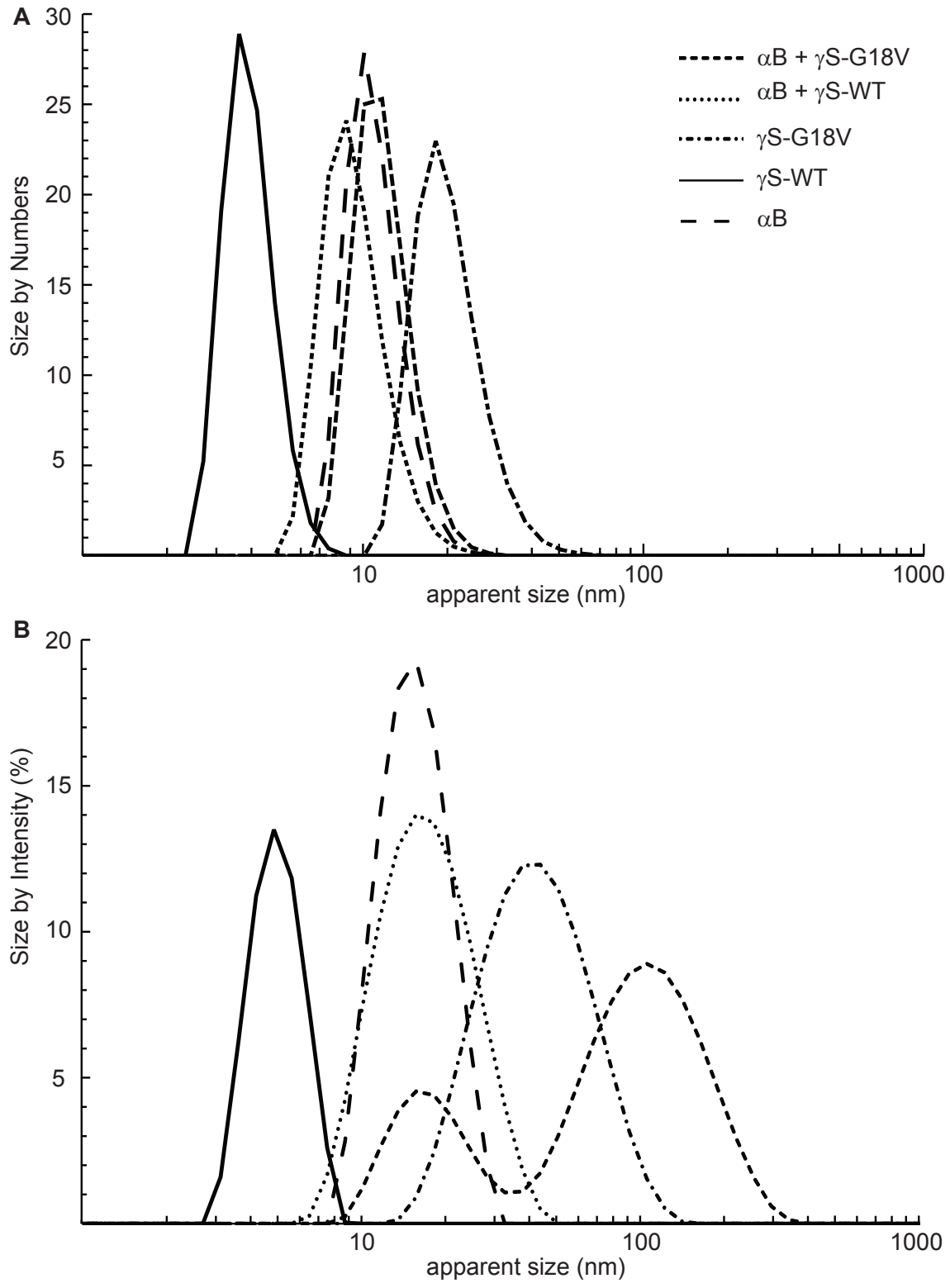

Figure S5: DLS data of αB, γS-WT, γS-G18V and mixtures thereof in 10 mM phosphate buffer pH 6.9 where (A) is the distribution of particle size by number and (B) is the distribution of particle size by intensity. The concentrations of the γS-WT, γS-G18V, and the αB samples are at 1.5 mM while the mixtures with αB consist of a 2:1 molar ratio of αB:γS. Both sets of data show that γS-G18V forms large aggregates at pH 6.9 and that the αB/γS-G18V mixture forms larger aggregates than that of either the αB-only and αB/γS-WT samples. Related to Figure 2.

Table S1: γS-WT RDCs. Related to Figure 1 and Table 1.

Res	D (Hz)	Res	D (Hz)	Res	D (Hz)	Res	D (Hz)
2	1.7	41	17.5	83	16.1	127	-27.9
3	3.9	42	-22.7	84	17.9	129	21.2
4	-14.4	43	24.6	85	20.2	130	17.5
5	-9.2	44	22.9	86	1.1	134	14.0
6	12.2	45	14.5	87	7.6	137ϵ	24.1
7	12.9	46	7.0	88	-28.0	138	-22.7
8	20.9	47	21.4	90	14.3	139	2.7
9	17.6	47ϵ	-27.1	91	-1.4	140	-26.0
10	13.2	48	17.6	92	-9.9	141	-22.7
11	-9.5	49	6.3	93	12.0	142	-22.7
12	-21.1	50	-12.2	94	-26.3	144	-34.0
13	-10.3	51	-30.1	96	18.4	145	-41.4
14	9.4	52	-35.8	97	0.3	146	-40.2
15	-35.6	54	-23.2	99	-27.9	147	-29.8
16	-28.3	55	-11.9	100	-19.2	148	4.4
17	-11.9	56	-42.8	101	11.2	150	-1.1
18	-27.8	57	-27.6	102	16.3	151	3.6
19	20.9	58	-9.6	104	-27.6	152	-22.7
20	19.7	61	0.8	105	-17.3	156	-22.7
21	1.1	62	20.1	106	-20.3	158	-6.5
22	-7.9	64	-10.6	107	20.3	159	-23.4
23	21.3	65	6.2	108	-32.2	161	-20.6
24	15.6	66	16.4	109	-10.9	162	-35.4
25	3.0	67	-27.0	110	-12.5	163	-0.3
26	2.7	69	-27.8	111	8.1	163ϵ	20.9
27	-22.7	70	-16.6	112	-11.8	164	-4.1
28	-31.9	71	-27.4	113	-20.3	165	-17.4
29	8.5	72	-33.0	114	10.5	166	-14.0
30	-14.1	73	-2.3	115	-6.9	167	3.5
31	-30.8	73ϵ	25.7	117	5.7	169	5.1
32	-6.0	74	-3.9	118	-20.6	170	-34.9
33	-42.5	75	-11.2	119	-36.7	171	23.5
34	-18.7	76	14.2	120	-42.1	172	13.1
35	-24.3	77	21.0	121	-26.7	173	14.8
36	-1.3	78	15.8	122	-29.3	174	25.3
37	-11.9	79	-15.4	123	-2.1	175	-5.9
38	-10.4	80	-40.1	124	-6.1	176	3.2
39	23.2	81	-45.2	125	-21.0	177	9.6
40	23.9	82	16.4	126	-34.9	178	-2.4

Table S2: γS-G18V RDCs. Related to Figure 1 and Table 1.

Res	D (Hz)	Res	D (Hz)	Res	D (Hz)	Res	D (Hz)
2	2.6	43	24.6	85	22.3	127	-33.8
3	3.4	44	24.4	86	1.4	128	-35.1
4	-7.7	45	8.4	87	7.2	129	21.1
5	-16.3	46	9.1	88	-22.2	130	14.4
6	15.1	47	14.9	90	25.0	134	1.2
7	18.4	47ϵ	17.9	91	-4.6	137ϵ	14.3
8	24.1	48	21.0	92	-13.2	138	20.4
9	-13.4	49	1.5	93	13.5	139	-2.1
10	8.6	50	-21.7	94	11.2	140	-35.1
11	-23.1	51	-55.3	96	17.4	142	-20.3
12	-33.8	52	-34.7	97	-4.9	144	-45.4
13	10.6	54	-31.5	99	-29.4	145	-38.3
14	6.3	56	-49.1	100	-23.4	146	-46.4
16	-26.5	57	-34.5	101	13.0	147	-35.4
17	-14.1	58	1.6	102	16.5	148	-1.3
18	-25.1	61	2.8	104	-31.9	150	3.5
19	-25.5	62	35.8	105	-20.4	151	5.4
21	-45.7	64	-11.6	106	-25.0	159	-24.7
22	16.6	65	4.7	107	23.0	161	-25.8
23	22.1	66	17.5	108	-38.6	162	-41.4
24	14.1	67	2.8	109	-14.8	163	-2.3
25	-1.4	69	-20.3	110	-17.3	163ϵ	23.4
26	-3.2	70	-19.9	111	10.7	164	-6.5
27	7.4	71	-41.4	112	6.6	165	-21.8
29	-30.3	72	-39.8	113	-19.4	166	-18.8
30	-33.8	73	-5.0	114	19.0	167	2.9
31	-30.1	73ϵ	28.4	115	-10.2	169	5.5
32	-5.1	74	10.6	117	3.3	170	-39.9
33	-44.0	75	-12.7	118	-27.4	171	-45.8
34	-17.9	77	24.0	119	-39.9	172	12.3
35	-39.3	78	14.3	120	22.1	173	16.7
36	-16.7	79	-19.5	121	-41.1	174	9.2
37	-36.7	80	-29.2	122	-33.3	175	-10.7
38	-35.4	81	-55.9	123	-14.9	176	5.0
39	26.4	82	18.9	124	-6.5	177	12.8
40	10.4	83	18.1	125	-25.1	178	-5.1
41	25.2	84	16.9	126	-43.5		

Supplemental Experimental Procedures

Structure Calculations The structures for γS-WT and γS-G18V were refined using the full NOE restraint set, residual dipolar couplings, TALOS+ generated dihedral restraints, H-N-HA derived 3J couplings, and hydrogen-bonding data from the H-D exchange experiments. 100 structures were calculated from an extended conformation using high-temperature torsion angle dynamics, a simulated annealing, followed by a cartesian space energy minimization. The average of the 10 lowest-energy structures was calculated and used as a starting structure for a final 200-structure calculation using a simulated annealing and Cartesian space energy minimization. The 20 lowest-energy structures were used as the final structure family. (Supplementary Figures S1 and S2, Table 1).

Structure families are shown for γS-WT and γS-G18V in Supplementary Figures S1 and S2. In the γS-G18V structure, V18 does not swing out into the solvent, but instead remains buried within the surrounding loop. The first 17 residues of the structure are largely unaffected by the substitution, while the dihedral angles shift from $\phi = 73.7$ °, $\psi = -163.0$ ° for G18 to $\phi = 129.8$ °, $\psi = -134.3$ ° for V18. Consistent with the change in amide chemical shifts observed in γS-G18V, the R19 backbone dihedral angles are substantially changed from their wild-type configurations. The presence of V18 shifts the R19 dihedral angles from $\phi = -58.6$ °, $\psi = -177.2$ ° to $\phi = -110.5$ °, $\psi = 17.9$ °. The 180 ° change in the ψ angle of R19 disrupts the R20–C23 β-sheet and the disruption propagates down the backbone. The exact structural cause of the ψ-inversion may be from steric clashes between the V18 sidechain and R19 carbonyl or other effects early in the folding of γS-crystallin from the presence of the highly hydrophobic V18. Additional structural calculations indicate that the V18 side chain remains buried even upon exclusion of all distance restraints to V18 (Supplementary Figure S3 (top)), and the adoption of a favorable backbone dihedral angle configuration would require the elimination of restraints from several surrounding residues, producing an extensive structural disruption to the surrounding loop region that is not supported by the NMR data (Supplementary Figure S3 (bottom)).

Monomeric γS-WT and γS-G18V under NMR conditions Samples of natural abundance wild-type γS-crystallin (γS-WT), and the variant γS-G18V were prepared in the NMR sample buffers in concentrations comparable to those used in structural NMR experiments. Light scattering measurements performed on these samples (Supplementary Figure S4) indicated that both and γS-G18V were monomeric under these buffer conditions. γS-WT, γS-G18V, αB-crystallin and mixtures thereof were also prepared in 10 mM phosphate, pH 6.9 in concentrations comparable to those used in NMR binding experiments. Light scattering measurements were then performed on these samples (Supplementary Figure S5). See main text for discussion of data.

Supplementary Information: Preferential and specific binding of human αB-crystallin to cataract-related variant of γS-crystallin

Carolyn N. Kingsley[†], William D. Brubaker[†], Stefan Markovic, Amanda J. Brindley, Anne Diehl, Hartmut Oschkinat & Rachel W. Martin[‡]

Supplemental Data

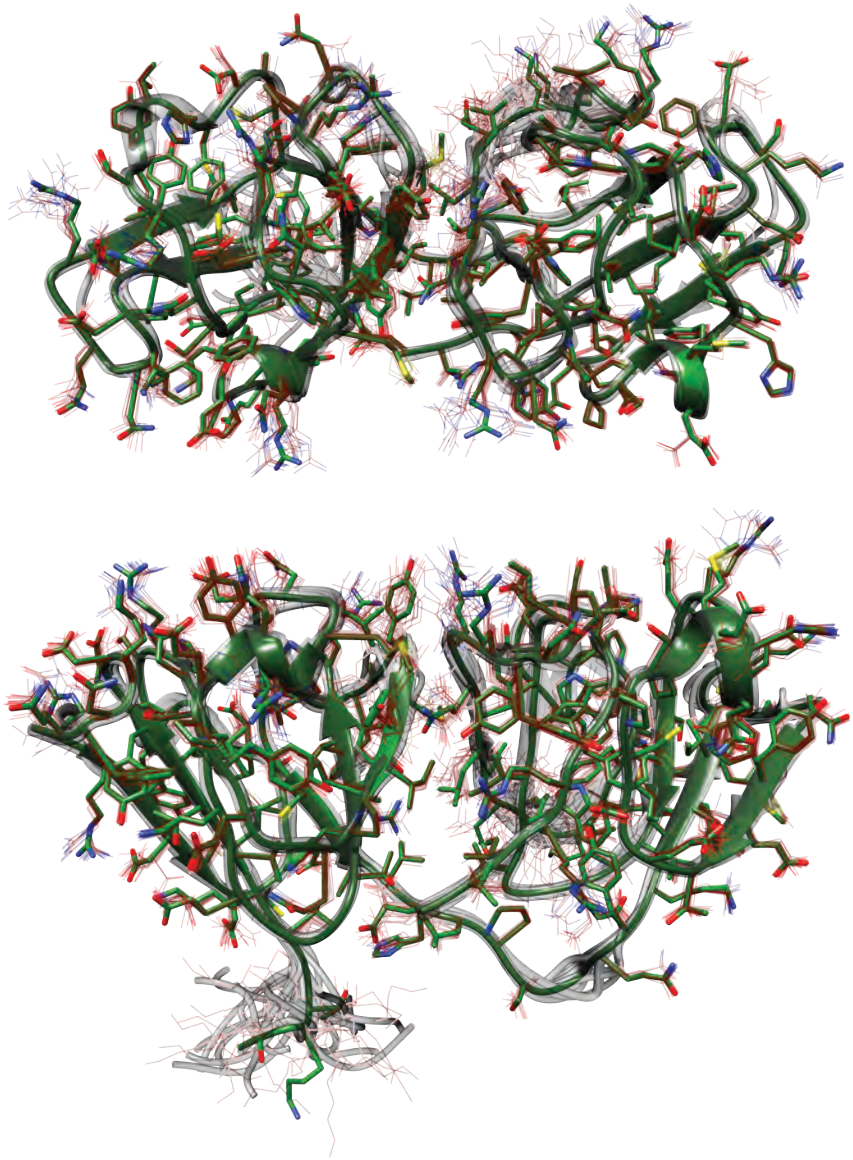

Figure 1: Depiction of the final 20-structure family for γS-WT (transparent grey, colored by heteroatom) and the energy-minimized average NMR structure (opaque green colored by heteroatom), including sidechains. Related to Figure 1 and Table 1.

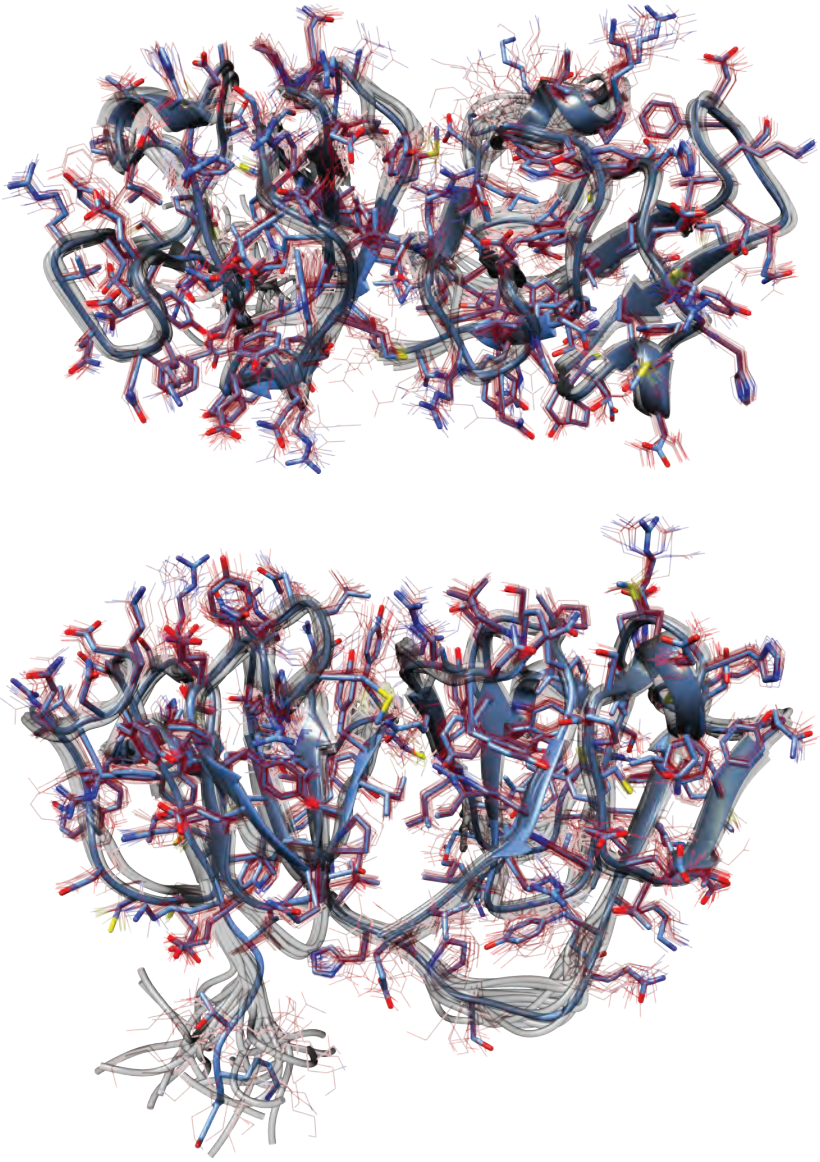

Figure 2: Depiction of the final 20-structure family for γS-G18V (transparent grey, colored by heteroatom) and the energy-minimized average NMR structure (opaque blue colored by heteroatom), including sidechains. Related to Figure 1 and Table 1.

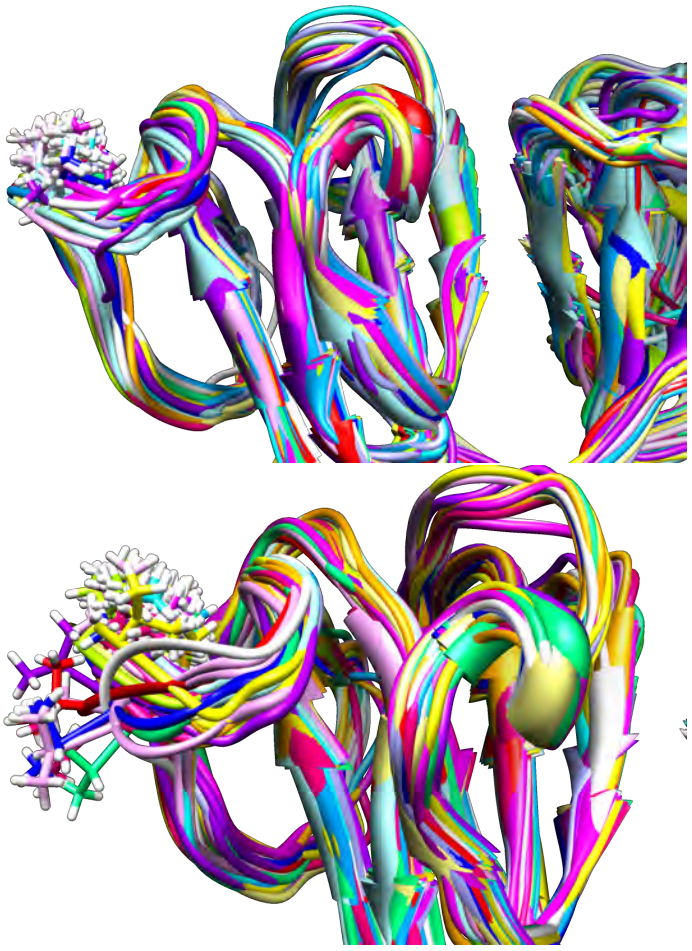

Figure 3: Comparison of two structural refinements without NOE restraints to residues 16-20 and without angular RDC restraints to residue 18 performed with (top) and without (bottom) the angular backbone restraint provided from the HNHA experiment for V18. Note that this single restraint is sufficient to keep V18 in place in all of the top scoring structures. Even if the J-coupling restraint is omitted, only five of 50 calculated structures land with V18 in an "allowed" dihedral angle conformation. Related to Figure 1 and Table 1.

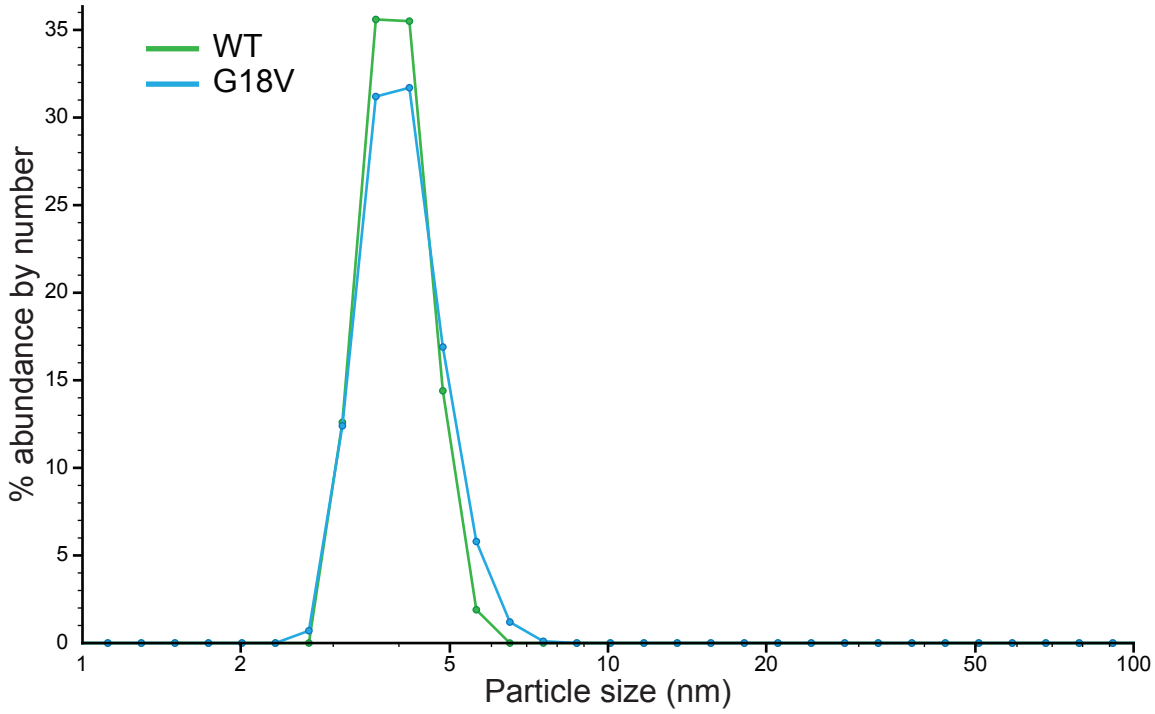

Figure 4: Particle size of γS-WT and γS-G18V at 2.0 mM concentration in 10 mM acetate buffer pH 4.5 measured by dynamic light scattering on a Zetasizer Nano ZS (Malvern Instruments, Ltd.). Under these conditions γS-WT and γS-G18V are fully monomeric, with particle diameters of 39.7 and 40.9 Å respectively. Related to Figure 1 and Table 1.

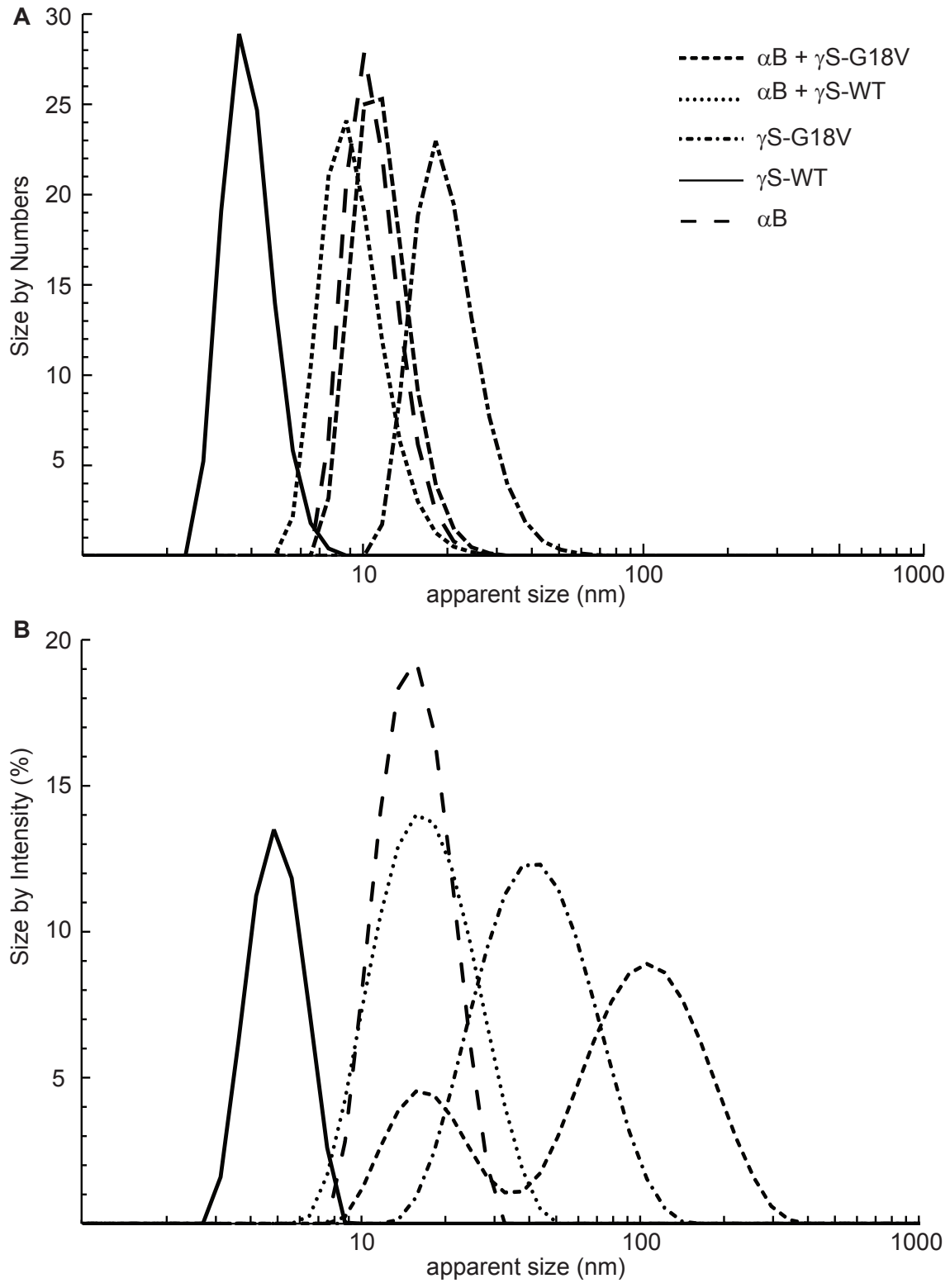

Figure 5: DLS data of αB, γS-WT, γS-G18V and mixtures thereof in 10 mM phosphate buffer pH 6.9 where (A) is the distribution of particle size by number and (B) is the distribution of particle size by intensity. The concentrations of the γS-WT, γS-G18V, and the αB samples are at 1.5 mM while the mixtures with αB consist of a 2:1 molar ratio of αB:γS. Both sets of data show that γS-G18V forms large aggregates at pH 6.9 and that the αB/γS-G18V mixture forms larger aggregates than that of either the αB-only and αB/γS-WT samples. Related to Figure 2.

Table 1: γS-WT RDCs. Related to Figure 1 and Table 1.

Res	D (Hz)	Res	D (Hz)	Res	D (Hz)	Res	D (Hz)
2	1.7	41	17.5	83	16.1	127	-27.9
3	3.9	42	-22.7	84	17.9	129	21.2
4	-14.4	43	24.6	85	20.2	130	17.5
5	-9.2	44	22.9	86	1.1	134	14.0
6	12.2	45	14.5	87	7.6	137ϵ	24.1
7	12.9	46	7.0	88	-28.0	138	-22.7
8	20.9	47	21.4	90	14.3	139	2.7
9	17.6	47ϵ	-27.1	91	-1.4	140	-26.0
10	13.2	48	17.6	92	-9.9	141	-22.7
11	-9.5	49	6.3	93	12.0	142	-22.7
12	-21.1	50	-12.2	94	-26.3	144	-34.0
13	-10.3	51	-30.1	96	18.4	145	-41.4
14	9.4	52	-35.8	97	0.3	146	-40.2
15	-35.6	54	-23.2	99	-27.9	147	-29.8
16	-28.3	55	-11.9	100	-19.2	148	4.4
17	-11.9	56	-42.8	101	11.2	150	-1.1
18	-27.8	57	-27.6	102	16.3	151	3.6
19	20.9	58	-9.6	104	-27.6	152	-22.7
20	19.7	61	0.8	105	-17.3	156	-22.7
21	1.1	62	20.1	106	-20.3	158	-6.5
22	-7.9	64	-10.6	107	20.3	159	-23.4
23	21.3	65	6.2	108	-32.2	161	-20.6
24	15.6	66	16.4	109	-10.9	162	-35.4
25	3.0	67	-27.0	110	-12.5	163	-0.3
26	2.7	69	-27.8	111	8.1	163ϵ	20.9
27	-22.7	70	-16.6	112	-11.8	164	-4.1
28	-31.9	71	-27.4	113	-20.3	165	-17.4
29	8.5	72	-33.0	114	10.5	166	-14.0
30	-14.1	73	-2.3	115	-6.9	167	3.5
31	-30.8	73ϵ	25.7	117	5.7	169	5.1
32	-6.0	74	-3.9	118	-20.6	170	-34.9
33	-42.5	75	-11.2	119	-36.7	171	23.5
34	-18.7	76	14.2	120	-42.1	172	13.1
35	-24.3	77	21.0	121	-26.7	173	14.8
36	-1.3	78	15.8	122	-29.3	174	25.3
37	-11.9	79	-15.4	123	-2.1	175	-5.9
38	-10.4	80	-40.1	124	-6.1	176	3.2
39	23.2	81	-45.2	125	-21.0	177	9.6
40	23.9	82	16.4	126	-34.9	178	-2.4

Table 2: γS-G18V RDCs. Related to Figure 1 and Table 1.

Res	D (Hz)	Res	D (Hz)	Res	D (Hz)	Res	D (Hz)
2	2.6	43	24.6	85	22.3	127	-33.8
3	3.4	44	24.4	86	1.4	128	-35.1
4	-7.7	45	8.4	87	7.2	129	21.1
5	-16.3	46	9.1	88	-22.2	130	14.4
6	15.1	47	14.9	90	25.0	134	1.2
7	18.4	47ϵ	17.9	91	-4.6	137ϵ	14.3
8	24.1	48	21.0	92	-13.2	138	20.4
9	-13.4	49	1.5	93	13.5	139	-2.1
10	8.6	50	-21.7	94	11.2	140	-35.1
11	-23.1	51	-55.3	96	17.4	142	-20.3
12	-33.8	52	-34.7	97	-4.9	144	-45.4
13	10.6	54	-31.5	99	-29.4	145	-38.3
14	6.3	56	-49.1	100	-23.4	146	-46.4
16	-26.5	57	-34.5	101	13.0	147	-35.4
17	-14.1	58	1.6	102	16.5	148	-1.3
18	-25.1	61	2.8	104	-31.9	150	3.5
19	-25.5	62	35.8	105	-20.4	151	5.4
21	-45.7	64	-11.6	106	-25.0	159	-24.7
22	16.6	65	4.7	107	23.0	161	-25.8
23	22.1	66	17.5	108	-38.6	162	-41.4
24	14.1	67	2.8	109	-14.8	163	-2.3
25	-1.4	69	-20.3	110	-17.3	163ϵ	23.4
26	-3.2	70	-19.9	111	10.7	164	-6.5
27	7.4	71	-41.4	112	6.6	165	-21.8
29	-30.3	72	-39.8	113	-19.4	166	-18.8
30	-33.8	73	-5.0	114	19.0	167	2.9
31	-30.1	73ϵ	28.4	115	-10.2	169	5.5
32	-5.1	74	10.6	117	3.3	170	-39.9
33	-44.0	75	-12.7	118	-27.4	171	-45.8
34	-17.9	77	24.0	119	-39.9	172	12.3
35	-39.3	78	14.3	120	22.1	173	16.7
36	-16.7	79	-19.5	121	-41.1	174	9.2
37	-36.7	80	-29.2	122	-33.3	175	-10.7
38	-35.4	81	-55.9	123	-14.9	176	5.0
39	26.4	82	18.9	124	-6.5	177	12.8
40	10.4	83	18.1	125	-25.1	178	-5.1
41	25.2	84	16.9	126	-43.5		

Supplemental Experimental Procedures

Structure Calculations The structures for γS-WT and γS-G18V were refined using the full NOE restraint set, residual dipolar couplings, TALOS+ generated dihedral restraints, H-N-HA derived 3J couplings, and hydrogen-bonding data from the H-D exchange experiments. 100 structures were calculated from an extended conformation using high-temperature torsion angle dynamics, a simulated annealing, followed by a cartesian space energy minimization. The average of the 10 lowest-energy structures was calculated and used as a starting structure for a final 200-structure calculation using a simulated annealing and Cartesian space energy minimization. The 20 lowest-energy structures were used as the final structure family. (Supplementary Figures S1 and S2, Table 1).

Structure families are shown for γS-WT and γS-G18V in Supplementary Figures S1 and S2. In the γS-G18V structure, V18 does not swing out into the solvent, but instead remains buried within the surrounding loop. The first 17 residues of the structure are largely unaffected by the substitution, while the dihedral angles shift from $\phi = 73.7$ °, $\psi = -163.0$ ° for G18 to $\phi = 129.8$ °, $\psi = -134.3$ ° for V18. Consistent with the change in amide chemical shifts observed in γS-G18V, the R19 backbone dihedral angles are substantially changed from their wild-type configurations. The presence of V18 shifts the R19 dihedral angles from $\phi = -58.6$ °, $\psi = -177.2$ ° to $\phi = -110.5$ °, $\psi = 17.9$ °. The 180 ° change in the ψ angle of R19 disrupts the R20–C23 β-sheet and the disruption propagates down the backbone. The exact structural cause of the ψ-inversion may be from steric clashes between the V18 sidechain and R19 carbonyl or other effects early in the folding of γS-crystallin from the presence of the highly hydrophobic V18. Additional structural calculations indicate that the V18 side chain remains buried even upon exclusion of all distance restraints to V18 (Supplementary Figure S3 (top)), and the adoption of a favorable backbone dihedral angle configuration would require the elimination of restraints from several surrounding residues, producing an extensive structural disruption to the surrounding loop region that is not supported by the NMR data (Supplementary Figure S3 (bottom)).

Monomeric γS-WT and γS-G18V under NMR conditions Samples of natural abundance wild-type γS-crystallin (γS-WT), and the variant γS-G18V were prepared in the NMR sample buffers in concentrations comparable to those used in NMR experiments. Light scattering measurements performed on these samples (Supplementary Figure S4) indicated that both and γS-G18V were monomeric under these buffer conditions.